Electromigration tuning of the voltage modulation depth in YBa2Cu3O7-delta nanowire-based SQUIDs

(article starts on next page)

Electromigration tuning of the voltage modulation depth in YBa$_2$Cu$_3$O$_{7-\delta}$ nanowire-based SQUIDs

E Trabaldo, **A Garibaldi**, **F Lombardi** and **T Bauch**[*]

Quantum Device Physics Laboratory, Department of Microtechnology and Nanoscience, Chalmers University of Technology, SE-41296 Göteborg, Sweden

E-mail: thilo.bauch@chalmers.se

Abstract

Oxygen electromigration applied to a YBa$_2$Cu$_3$O$_{7-\delta}$ nanowire can be used to tune its electrical properties. Here, we apply electromigration to YBCO nanowire-based superconducting quantum interference devices (SQUIDs) and study its effect on the voltage modulation depth of the devices. Using a dc electromigration current we replenish the oxygen of the weak links, improving the critical current symmetry of the SQUIDs. AC current electromigration is used to reduce the doping level of the weak links, thus reducing their critical current and increasing differential resistance. Both type of electromigration processes are found to improve the SQUIDs performance, although the best results are obtained with ac biased electromigration, which improved the voltage modulations of the SQUIDs by a factor as high as 8. This procedure can be instrumental to fine tune ex-situ the properties of superconducting electronics where a large number of weak links are required.

Keywords: YBCO, SQUID, HTS, nanowire, electromigration

(Some figures may appear in colour only in the online journal)

1. Introduction

Superconducting quantum interference devices (SQUIDs) are one of the main technological application of superconductors, being utilized, among others, in biomagnetic diagnostics, scanning SQUID microscopy, and geophysical surveys [1–4]. High critical temperature superconductor (HTS) based SQUIDs can be operated at liquid nitrogen temperatures, simplifying the cryogenic requirements as compared to low temperature superconductor (LTS) based SQUIDs, which instead relies on scarce and expensive liquid He.

The state-of-the-art HTS based SQUIDs operating at 77 K implement grain boundary (GB) based Josephson junctions, such as bicrystal or step-edge junctions [5–10]. While the performances of GB-based SQUIDs have opened the doors to HTS technological applications, their fabrication is challenging, requiring several lithography steps in the case of step edge GB junctions [7, 11, 12]. Moreover, in the case of bicrystal junctions the number of junctions per chip and the design flexibility is limited due to the location of the junctions along the bicrystal GB line.

HTS YBa$_2$Cu$_3$O$_{7-\delta}$ (YBCO) nanowires have been proposed as an alternative to GB-based junctions [13, 14]. They can be realized using a single lithography step, placed anywhere and freely oriented within the film plane. However, the large critical current densities and fluctuations of critical currents for nominally identical nanowires [15] limit the performance of YBCO nanowire based SQUIDs. The asymmetry of the critical currents of the two nanowires and the large

---

[*] Author to whom any correspondence should be addressed.

screening parameter $\beta_L = I_{SQ}L_{SQ}/\Phi_0$, with I_{SQ} the SQUID critical current, L_{SQ} the SQUID inductance, and Φ_0 the superconductive flux quantum, result in degradation of the SQUID voltage modulation depth ΔV, thereby increasing the overall flux noise of the SQUID $S_\Phi^{1/2} \propto 1/\Delta V$ [14].

Tuning the hole doping of YBCO through electromigration (EM) of oxygen was first studied for thin films [16] and GB junctions [17], and it has seen recent advancements also for YBCO micro bridges [18, 19] and nanowires [20]. These developments open up the possibility to modify ex-situ the electrical properties of YBCO nanowire based SQUIDs, similarly to the work on EM of LTS-based SQUIDs [21]. Here, applying a dc current density (DC-EM) in the range $7–15 \text{ MA cm}^{-2}$ to a YBCO nanowire increases the hole doping [20]. Increasing the current density above 15 MA cm^{-2} causes a reduction of the doping, although with a rather inhomogeneous doping distribution along the wire. A more controlled way to reduce the hole doping can be achieved by applying an ambipolar square wavefunction at 1 kHz (AC-EM) with amplitude above 17 MA cm^{-2} [20]. Since the zero temperature critical current and critical temperature of a nanowire depends on its doping level, EM can be used to tune the electrical properties of the nanowires in a SQUID, and therefore adjust for optimal operation at e.g. 77 K.

In this work we explore the effects of EM on the voltage modulations of YBCO nanowire-based SQUIDs. Here, we use the different effects of DC vs AC biasing to address two of the main limitations of such SQUIDs: (1) asymmetry of the critical currents of the individual weak links, which results in reduced critical current modulations. Here DC-EM is used to replenish oxygen in the weak links, thereby reducing the asymmetry of the critical currents. (2) High values of the SQUID critical current, which results in increased screening parameter. Here, AC-EM is used to reduce the critical current of the SQUIDs. These findings could be easily applied to other types of HTS weak links such as the grooved Dayem bridge [22] for the ex-situ optimization of HTS based electronics.

2. SQUIDs fabrication and design

All the data reported here have been obtained from SQUIDs fabricated on a SrTiO$_3$ substrate. A 50 nm thick thin film of YBCO is deposited on the substrate by pulsed laser deposition (PLD) and after covered by a 100 nm thick layer of amorphous carbon, also deposited by PLD. The carbon mask is defined by electron beam lithography, followed by lift-off and reactive ion etching in oxygen plasma. A subsequent Ar$^+$ ion milling process transfers the pattern into the YBCO film. Details about the fabrication process, resulting in high-quality YBCO nanowires with pristine bulk-like properties down to cross-section of 50 nm×50 nm are reported in references [15, 23].

In figure 1(a) we show a scanning electron microscope (SEM) image of a nanowire-based SQUID. The top and bottom electrodes are connected to a signal generator, which provides the SQUID bias current i_{SQ}, and to a low noise amplifier, which measures the voltage drop V over the SQUID.
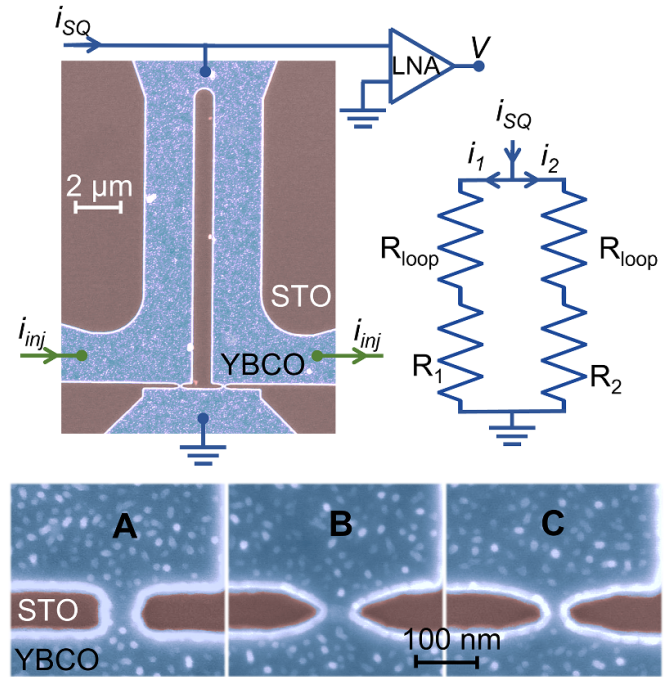

Figure 1. False color scanning electron microscope (SEM) image of a SQUID connected to the measurement setup and its equivalent circuit in the normal state (above critical temperature). The bottom SEM images show a comparison of the different geometries (A, B and (C) used for the weak links.

The SQUID loop is additionally connected to a second current source, which is used for current injection i_{inj} to modulate the phase difference between the two nanowires $\Delta\varphi = L_{loop}i_{inj}2\pi/\Phi_0$ [24].

The configuration shown in figure 1 is also used for the EM of the weak links, where the EM current is i_{SQ}. An equivalent circuit of the SQUID in its normal state, i.e. above the critical temperature $T > T_c$, is also shown in figure 1. Given the macroscopic size (several μm) of the arms of the SQUID loop, one can assume that the values of the electrical resistance of the two SQUID arms are the same and equal to R_{loop}. On the other hand, the resistance of the two nanowires, R_1 and R_2, could differ since we are approaching the limits of the fabrication process. The current i_{SQ} is divided in the two arms of the SQUID according to Kirchhoff's circuit laws. If $R_1 = R_2$, then $i_1 = i_2 = i_{SQ}/2$, where $i_{1,2}$ is the current in the two arms of the SQUID. On the other hand, if $R_1 > R_2$, then $i_1 < i_2$, and vice versa. This results in the parallel EM of the two weak links. This process has been studied in details with two or more weak links for the fabrication of nanogaps [25–27] and has been recently used for LTS constriction-based SQUIDs [28, 29].

Since the EM is strongly influenced by the value of local current density, regions of the device with constrictions and current crowding effects are affected more strongly by the EM process. The geometry of the nanowire can be designed to take advantage of this effects. We fabricated SQUIDs based on weak links with three different geometrical profiles, labeled A, B and C; in figure 1 are compared the SEM images of the three types of weak link. Type A are rectangular shaped nanowires

Table 1. Summary of the values of critical current and voltage modulation depth measured at 80 K on SQUID SQA, SQB, and SQC, before and after the different EM steps.

	Before EM		DC		AC1		AC2	
	I_c μA	ΔV μV	I_c μA	ΔV μV	I_c μA	ΔV μV	I_c μA	ΔV μV
SQA	580	—	550	0.2	190	1	110	1.7
SQB	700	—	700	0.7	610	1.5	330	1.8
SQC	500	0.7	510	0.7	150	5	100	4.7

with a 2:1 aspect ratio, while type B and C are designed with constrictions to limit the effect of the EM to small region (narrowest section) of the weak link. The latter two geometries have also the advantage of reducing the overall parasitic kinetic inductance of the weak links.

3. Results and discussion

In the following we focus on the results obtained for three SQUIDs: SQA, SQB, and SQC. Those SQUIDs have each a different type of weak link (A, B and C respectively) and have been selected to compare the effects of EM on the different weak link geometries.

To study the effect of the EM on the performance of the SQUIDs, we monitor the voltage modulation depth ΔV while repeating the same EM steps on all the SQUIDs and characterizing them at 80 K before and after each step. All the EM steps reported in this work, both DC and AC, were performed in a He atmosphere with a pressure of $\simeq$200 mbar. First, the SQUIDs critical current and voltage modulation depth are measured directly after fabrication (before EM in table 1). Thereafter, DC-EM is performed at room temperature; for this step a DC current bias is applied to the SQUID and manually increased.

The effect of DC-EM is to replenish the nanowires with oxygen, and the aim of this step is to heal regions with suppressed superconductivity due to possible oxygen loss during the nano fabrication process. At the same time, this will improve the critical current symmetry of the weak links. The DC bias current is increased to $i_{SQ} \simeq 3$ mA, which is the maximum value above which the doping starts to decrease again. This maximum current corresponds to a current density of $\simeq$15 MA cm^{-2}, which is consistent with previous values reported for DC-EM in YBCO nanowires [20]. The SQUIDs are then characterized after the DC-EM (DC in table 1).

The successive steps of AC-EM (labeled AC1 and AC2), aimed at reducing the critical current of the weak links, are performed at liquid nitrogen temperature using a square wavefunction centered around zero with frequency of 1 kHz. An estimation of the diffusion relaxation time gives $\tau = l^2/(2\pi^2 D) \simeq 400$ s, using the following expression for the diffusion constant $D = 1.4 \times 10^{-8} \exp\left(-0.97 \text{ eV}/k_B T\right)$ [17], with k_B the Boltzmann constant and wire length $l = 400$ nm. Here we considered an elevated temperature of $T = 550$ K due to Joule heating during the EM process (estimated from the measured wire resistance under applied DC bias, which increases approximately linearly with temperature in the

optimal doping regime). Therefore, due to the large relaxation time constant, which is much larger than the period of the applied alternating current, oxygen is barely being displaced by the applied potential difference on the length scale of the nanowire. Instead, the dominant process responsible for moving oxygen away from the wire is given by thermomigration [30]. Here the large temperature gradient between the wire and the electrodes dominates the oxygen migration process in YBCO nanowires.

During AC-EM, the bias current is applied in bursts of 100 ms duration. Between each burst the AC current is turned off and the zero bias resistance (applied currents much smaller than the ones used for the oxygen migration process) of the wire is measured.

In figures 2(a)–(c) are shown the current–voltage characteristics (IVC) of the three SQUIDs before and after the EM steps, while in figures 2(d)–(f) are shown the corresponding voltage modulations versus normalized applied magnetic flux. The voltage modulations of SQA and SQB before EM are not reported since their amplitude was below the noise limit of our experimental set-up. Similar results have been obtained for all SQUIDs based on nanowires type A and B. Only SQUID SQC, based on type C weak links, shows small voltage modulations already before any EM processing.

After DC-EM, the voltage modulation depths ΔV of SQA and SQB are increased above the noise level of the measurement system. We attribute this increase mainly to an improved critical current symmetry of the weak links after DC-EM. However, for SQA we cannot rule out the effect of increased differential resistance close to the critical current (see figure 2(a)). For SQC, the DC-EM step has no measurable effect on ΔV, suggesting that the critical current values of the weak links were already comparable after fabrication.

On the other hand, one can see a drastic change in both the IVCs and voltage modulations of the SQUIDs after each AC-EM step. The main effects of AC-EM are the reduction of the critical current while the differential resistance is increased (see figure 2). These result in a further increase of voltage modulations, up to a factor 8 for SQA and a factor 7 for SQC. The voltage modulations of SQB improves only by a factor 2, this is mainly limited by how low the critical current could be reduced. Indeed, for type B weak links I_c could only be reduced by a factor $\simeq$2, before the weak links would degrade very fast and lose all superconducting properties. AC-EM in weak links of type B is confined to the central constriction, especially to the inner corners where current crowding is enhanced. This results in critically high electric field and
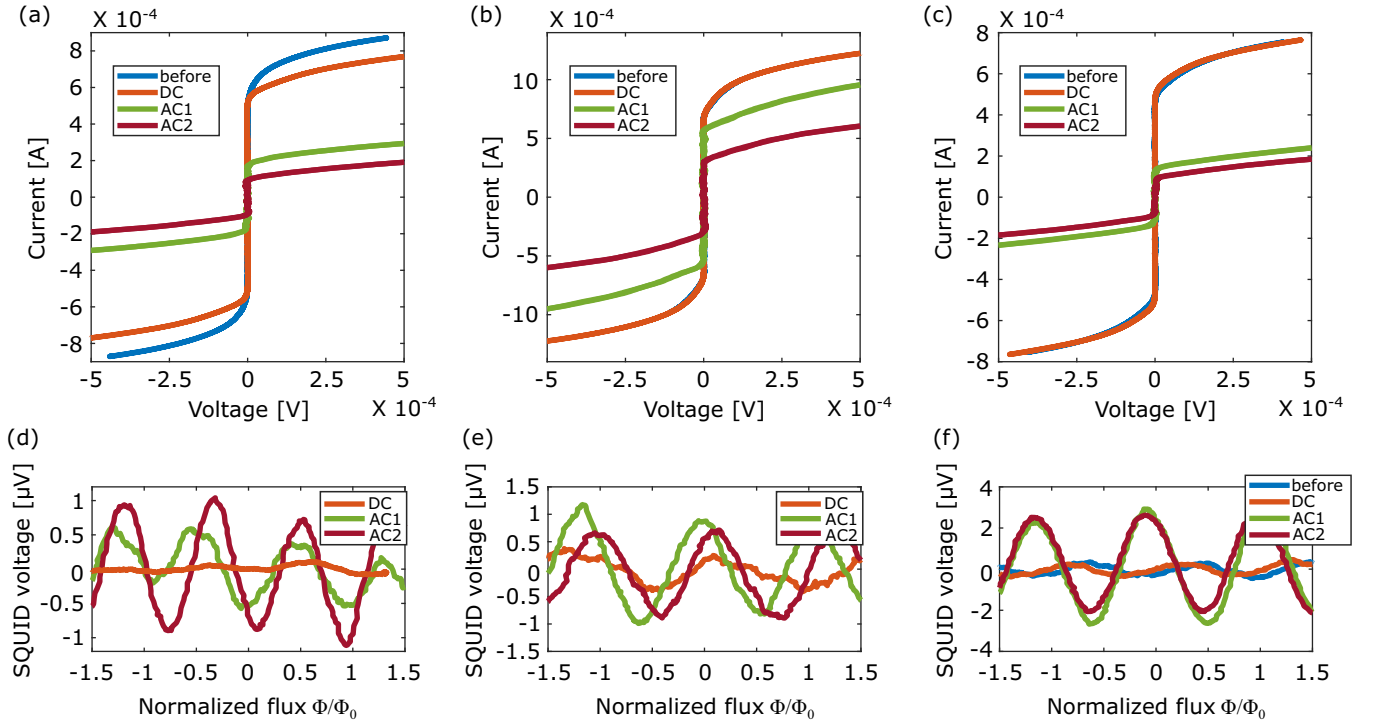
Figure 2. Current–voltage characteristics measured at 80 K before and after different EM steps on SQA (a), SQB (b), and SQC (c). SQUID voltage modulations versus normalized magnetic flux, measured at 80 K before and after different EM steps on SQA (d), SQB (e), and SQC (f). Note, the observed shift of the voltage modulations in panels (d)–(f), i.e. the voltage modulations not being centered around zero flux, after AC-EM is most probably caused by flux trapping. The EM process locally heats the weak links well above the critical temperature promoting flux trapping in regions of the SQUIDs, which reach temperatures close to T_C of the film during the EM process.

limits the control over the AC-EM process. Any further step of AC-EM on SQB would result in thermal runaway and irreversible damaging of the weak links. Weak links C have a similar constriction profile, however the central part is designed to be longer to avoid the limitations, such as current crowding, of weak links of type B.

In the following we analyze the evolution of the voltage modulation depth ΔV after each AC-EM step using the following expression derived for SQUIDs implementing equal resistively shunted Josephson junctions (RSJ) [31]

$$\Delta V = \frac{4}{\pi} \frac{I_c R_n}{1 + \beta_L} \exp\left(-3.5\pi^2 \frac{k_B T L_{SQ}}{\Phi_0^2}\right) \quad (1)$$

where R_n is the normal resistance of the SQUID, k_B is the Boltzman constant, L_{SQ} the SQUID inductance. While our weak links are not in the limit of the RSJ-model, equation (1) can be used as a first approximation to study the evolution of ΔV after AC-EM.

The SQUID inductance L_{SQ} can be written as $L_{SQ} = L_{loop} + 2L_{wl}$, where L_{loop} and L_{wl} are the inductance of the SQUID hairpin loop and of a weak link respectively. The former can be calculated as $L_{loop} = \Phi_0/I_{mod}$, where I_{mod} is the value of injection current needed to obtain a full modulation of the SQUID voltage. For our SQUID we measured $I_{mod} = 48 \ \mu A$, which results in $L_{loop} = 42$ pH. Since AC-EM affects only the nanowires, L_{loop} remains constant. On the other hand, the nanowire inductance is dominated by kinetic inductance

and can be calculated as $L_{wl} = \mu_0 \lambda^2 l/wt$, thus L_{wl} is strongly affected by a change in T_c.

The main effect of AC-EM is to reduce the nanowire doping, which influences the critical temperature T_c, London penetration depth and coherence length of the weak link. However, the most relevant effect in our case is the reduction of the critical temperature T_c, since the properties of YBCO change drastically at temperatures close to T_c. In our case, we are maintaining the temperature of the SQUIDs at 80 K, while instead lowering the T_c of the weak links through EM.

One can calculate the values of the London penetration depth and of the critical current as a function of T_c as

$$I_c(T_c) = I_c^0 \left(1 - \left(\frac{T}{T_c}\right)^2\right)^{3/2} \quad (2)$$

$$\lambda(T_c) = \lambda^0 \left(1 - \left(\frac{T}{T_c}\right)^n\right)^{-1/2} \quad (3)$$

where equation (2) is the Bardeen expression for the depairing critical current of nanowires [15, 32], $n \simeq 2$ is a typical exponent for YBCO , while I_c^0 and λ^0 are the values of critical current and London penetration depth in the limit $T = 0$. In the following we assume I_c^0 and λ^0 to be constant since their values do not change significantly in the range of doping we explore with EM.

One can use equation (1) to calculate the expected voltage modulations depth of SQA, SQB and SQC for different values
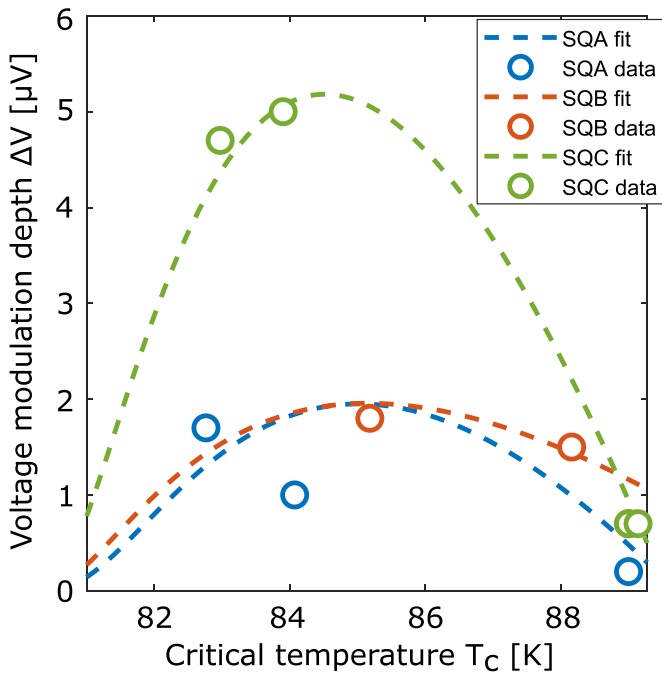
Figure 3. Comparison of the measured voltage modulation depths of SQA, SQB and SQC, and the corresponding values obtained using equation (1).

4. Conclusions

In this work we present a protocol to use EM to significantly improve the performances, in terms of voltage modulation depth, of nanowire-based SQUIDs operating at 80 K. Since the effects of the EM are strongly influenced by current crowding effects, we designed SQUIDs with three types of weak links. First, we used DC-EM to increase the doping of the weak links while also improving their critical current symmetry. This improved the ΔV of SQA and SQB, which could not be detected before DC-EM due to the measurements setup noise level. Subsequent AC-EM treatment steps are applied to reduce the doping level of the weak links, which results in lower critical currents and higher differential resistances. Here, an increase of the voltage modulation depth by a factor up to 8 could be achieved.

The highest values of ΔV are achieved for nanowires with a gradual narrowing of the central part (type C), where the increase of the kinetic inductance of the weak link is minimized during EM

Our findings can be extended to most HTS-based devices, where the EM of oxygen atoms determines their doping level. The results on the different weak link types suggest that this technique would be particularly well suited for constriction type weak links and grooved Dayem bridges [22], for which EM is expected to occur locally.

Data availability statement

The data that support the findings of this study are available upon reasonable request from the authors.

ORCID iDs

E Trabaldo https://orcid.org/0000-0002-0188-6814
F Lombardi https://orcid.org/ 0000-0002-3478-3766
T Bauch https://orcid.org/0000-0002-8918-4293

of the weak links critical temperature, i.e. for different doping levels. Here the critical temperatures of the weak links were determined by comparing the SQUIDs' critical currents to the Bardeen expression (see equation (2)). The normal resistances of our weak links cannot be extracted from the measured IVC, instead we set $R_n = R_d/k$, with R_d the value of the dynamical resistance at the working point, and k a fitting parameter. For a SQUID at 77 K in the limit of the RSJ-model, the fitting parameter is approximately 2.8 [33]. In figure 3 we show the measured voltage modulation depths (open symbols) for the three SQUIDs after each EM step together with the expected voltage modulation depth using equation (1). We find the best fitting of the measured ΔV by using $k = 5$ for SQA and SQB, and $k = 3.5$ for SQC.

For all three SQUIDs we find that ΔV first increases with decreasing critical temperature of the weak links. This can be understood from the reduction of the screening parameter and increase of the differential resistance with decreasing critical temperature (see equation (1)). However, for $T_c \leqslant$ 85 K the voltage modulations of the SQUIDs start decreasing again, even though β_L continues to decrease. However, when the T_c of the weak link reaches the bath temperature of 80 K the SQUID critical current drops to zero, causing the voltage modulation depth to go to zero as well (see equation (1)). Moreover, the largest modulation depth after EM can be achieved with nanowires with a gradual narrowing of the central part (see weak link of type C in figure 1, bottom). Here AC-EM most probably affects only the central part of the nanowire, while keeping the rest of the wire unaffected. This mitigates the increase of the kinetic inductance of the weak links of type C caused by the reduction of T_c as compared to wires of type A, where EM affects the whole length of the wire.

References

[1] Clarke J and Braginski A I 2006 *The Squid Handbook: Applications of Squids and Squid Systems* (New York: Wiley)
[2] Fagaly R 2006 *Rev. Sci. Instrum.* **77** 101101
[3] Seidel P 2015 *Applied Superconductivity: Handbook on Devices and Applications* (New York: Wiley)
[4] Granata C and Vettoliere A 2016 *Phys. Rep.* **614** 1–69
[5] Koelle D, Kleiner R, Ludwig F, Dantsker E and Clarke J 1999 *Rev. Mod. Phys.* **71** 631

[6] Faley M, Dammers J, Maslennikov Y, Schneiderman J, Winkler D, Koshelets V, Shah N and Dunin-Borkowski R 2017 *Supercond. Sci. Technol.* **30** 083001

[7] Mitchell E and Foley C 2010 *Supercond. Sci. Technol.* **23** 065007

[8] Öisjöen F, Schneiderman J F, Figueras G, Chukharkin M, Kalabukhov A, Hedström A, Elam M and Winkler D 2012 *Appl. Phys. Lett.* **100** 132601

[9] Nagel J *et al* 2010 *Supercond. Sci. Technol.* **24** 015015

[10] Beyers R *et al* 1989 *Nature* **340** 619–21

[11] Lombardi F, Ivanov Z, Fischer G, Olsson E and Claeson T 1998 *Appl. Phys. Lett.* **72** 249–51

[12] Hilgenkamp H and Mannhart J 2002 *Rev. Mod. Phys.* **74** 485

[13] Arpaia R, Arzeo M, Nawaz S, Charpentier S, Lombardi F and Bauch T 2014 *Appl. Phys. Lett.* **104** 072603

[14] Xie M, Chukharkin M, Ruffieux S, Schneiderman J, Kalabukhov A, Arzeo M, Bauch T, Lombardi F and Winkler D 2017 *Supercond. Sci. Technol.* **30** 115014

[15] Nawaz S, Arpaia R, Bauch T and Lombardi F 2013 *Phys. C* **495** 33–8

[16] Robbes D, Miklich A, Kingston J, Lerch P, Wellstood F and Clarke J 1990 *Appl. Phys. Lett.* **56** 2240–2

[17] Moeckly B, Lathrop D and Buhrman R 1993 *Phys. Rev. B* **47** 400

[18] Baumans X D, Fernández-Rodríguez A, Mestres N, Collienne S, Van de Vondel J, Palau A and Silhanek A V 2019 *Appl. Phys. Lett.* **114** 012601

[19] Marinković S *et al* 2020 *ACS nano* **14** 11765–74

[20] Trabaldo E, Kalaboukhov A, Arpaia R, Andersson E, Lombardi F and Bauch T 2021 Tuning the doping of $YBa_2Cu_3O_{7-\delta}$ nanowires through electromigration (Preprint 2105.13933)

[21] Collienne S, Raes B, Keijers W, Linek J, Koelle D, Kleiner R, Kramer R B, Van de Vondel J and Silhanek A V 2021 *Phys. Rev. Appl.* **15** 034016

[22] Trabaldo E, Pfeiffer C, Andersson E, Arpaia R, Kalaboukhov A, Winkler D, Lombardi F and Bauch T 2019 *Nano Lett.* **19** 1902–7

[23] Nawaz S, Arpaia R, Lombardi F and Bauch T 2013 *Phys. Rev. Lett.* **110** 167004

[24] Johansson J, Cedergren K, Bauch T and Lombardi F 2009 *Phys. Rev. B* **79** 214513

[25] Johnston D E, Strachan D R and Johnson A C 2007 *Nano Lett.* **7** 2774–7

[26] Zhang H, Thompson C, Stellacci F and Thong J 2010 *Nanotechnology* **21** 385303

[27] Johnson S L, Hunley D P, Sundararajan A, Johnson A C and Strachan D R 2010 *IEEE Trans. Nanotechnol.* **10** 806–9

[28] Keijers W, Baumans X D, Panghotra R, Lombardo J, Zharinov V S, Kramer R B, Silhanek A V and Van de Vondel J 2018 *Nanoscale* **10** 21475–82

[29] Lombardo J *et al* 2018 *Nanoscale* **10** 1987–96

[30] Oriani R 1969 *J. Phys. Chem. Solids* **30** 339–51

[31] Enpuku K, Shimomura Y and Kisu T 1993 *J. Appl. Phys.* **73** 7929–34

[32] Bardeen J 1962 *Rev. Mod. Phys.* **34** 667

[33] Enpuku K, Tokita G and Maruo T 1994 *J. Appl. Phys.* **76** 8180–5